Oceanologia 64 (2022) 327—345

Available online at www.sciencedirect.com

ScienceDirect

journal homepage: www.journals.elsevier.com/oceanologia

ORIGINAL RESEARCH ARTICLE

Numerical simulation of tidal hydrodynamics in the Arabian Gulf

Fawaz Madah[a,*], **Sameer H. Gharbi**[a,b]

[a] *Department of Marine Physics, Faculty of Marine Sciences, King Abdul-Aziz University, Jeddah, Saudi Arabia*
[b] *Department of Physical Oceanography, Faculty of Marine Sciences and Environment, Hodeidah University, Hodeidah, Yemen*

Received 28 August 2021; accepted 13 January 2022
Available online 31 January 2022

KEYWORDS
Arabian Gulf;
Delft3D;
Strait of Hormuz;
Amphidromic point;
Co-tidal charts

Abstract A vertically 2-D numerical model based on the *Delft3D* modelling system is set up, calibrated, and validated to simulate the tidal hydrodynamics in the Arabian Gulf. The model is a barotropic solution, controlled by 13 tidal components at open boundaries. The performance of the numerical model was evaluated using the hourly water level observations and the TOPEX/Poseidon altimetry data. Statistical analysis showed a good agreement between the simulated and observed water levels. *RMS* error was found to be ranged from 0.07 to 0.23 m, with maximum discrepancies observed at Ras Tanura and Mina Sulman stations. However, the *IOA* between the simulated and observed water levels was significant (0.95—0.99). On average, the errors for the tidal constituents considered in the analysis are in the order of <0.02 m (4%). The M_2, S_2, K_1 and O_1 tidal waves represent the largest among other constituents, where the amplitude of S_2 represents almost 30% of the M_2, and the O_1 tidal wave represents about 50% of the K_1 tide. The co-tidal charts of the semidiurnal tides show the existence of two anticlockwise amphidromic systems in the north and south ends (centred around 28.25° and 24.5°N respectively) close to the western side, while the diurnal constituents form only a single amphidromic point in the central part, centred around 26.8°N (North Bahrain). On the other hand, the velocity amplitudes of the *U* and *V* components of the numerical model were compared with a previous observational study and found to be agreed well.

* Corresponding author at: Department of Marine Physics, Faculty of Marine Sciences, King Abdulaziz University, Jeddah, Saudi Arabia.
E-mail address: fmaddah@kau.edu.sa (F. Madah).
Peer review under the responsibility of the Institute of Oceanology of the Polish Academy of Sciences.

Production and hosting by Elsevier

https://doi.org/10.1016/j.oceano.2022.01.002

1. Introduction

On the global level, the Arabian Gulf (AG) (known also as the Persian Gulf) is an important region environmentally, economically, and politically due to the oil-related activities and gas resources. The physical border of the AG is surrounded by the shoreline of Saudi Arabia, Bahrain, and Qatar on the western edge, the coastline of Iran on the eastern side, Kuwait in the north-western part, Iraq on the northern part, and the United Arab Emirates (UAE) on the southwestern coastline (Figure 1). Generally, the AG experiences a sub-tropical climate due to its location in the north of the tropic of cancer. A common weather event in the region is known as the "Shamal", which is a north-westerly wind predominant throughout the year (Perrone, 1979). However, the weather condition experiences seasonal variations connected with the amplitudes of the Arabian and Indian thermal lows (Emery, 1956; Perrone, 1979). The AG region is characterized by high evaporation rates ($\sim$ 2 m yr^{-1}) (Ahmad and Sultan, 1991; Privett, 1959) which exceed the net freshwater either by precipitation or rivers flow (Al-Subhi, 2010; Pous et al., 2012). As a result, the AG acts as a large inverse-estuarine system, where the Strait of Hormuz is the only mechanism that controls the exchange between the AG and the northern Indian Ocean. The physical and hydrographic conditions of the AG including water temperature, salinity, wind conditions, heat flux, flow exchange regime, etc, can be found in the previous investigations (e.g., Ahmad and Sultan, 1991; Al-Subhi, 2010; Brewer et al., 1978; Brewer and Dyrssen, 1985; Chao et al., 1992; Emery, 1956; Johns et al., 2003; Kämpf and Sadrinasab, 2006; Pous et al., 2004; Reynolds, 1993; Yao, 2008).

Tides in the AG are an important driving force (Elshorbagy et al., 2006). The tidal wave in the AG is to be oscillating at a period of 22.6 or 21.7 hours where the main tidal motion in the AG is due to Kelvin waves (Defant, 1961). Several studies were carried out in the AG to study the tidal conditions using tide gauge data (Akbari et al., 2016; Al-Mahdi et al., 2009; Al-Subhi, 2010; Khalilabadi, 2016; Sharaf El-Din, 1988; Siddig et al., 2019; Sultan et al., 1995). On the other hand, a number of modelling studies were applied to study the tidal components considering only the four principal tidal components (M_2, S_2, O_1, K_1), which considered for producing the amplitude and phase charts (Bashir, 1993; Lardner et al., 1982,1988; Poul et al., 2016; Najafi and Noye, 1997; Pous et al., 2012; Thompson et al., 1994; Trepka, 1968). The conclusion drawn from these studies suggests that the tidal system is complex and changes from being primarily semi-diurnal to diurnal throughout the basin. Interaction between semidiurnal (M_2, S_2) and diurnal (O_1, K_1) tidal constituents yield resonance, where the former results in two amphidromic systems (one in the north-

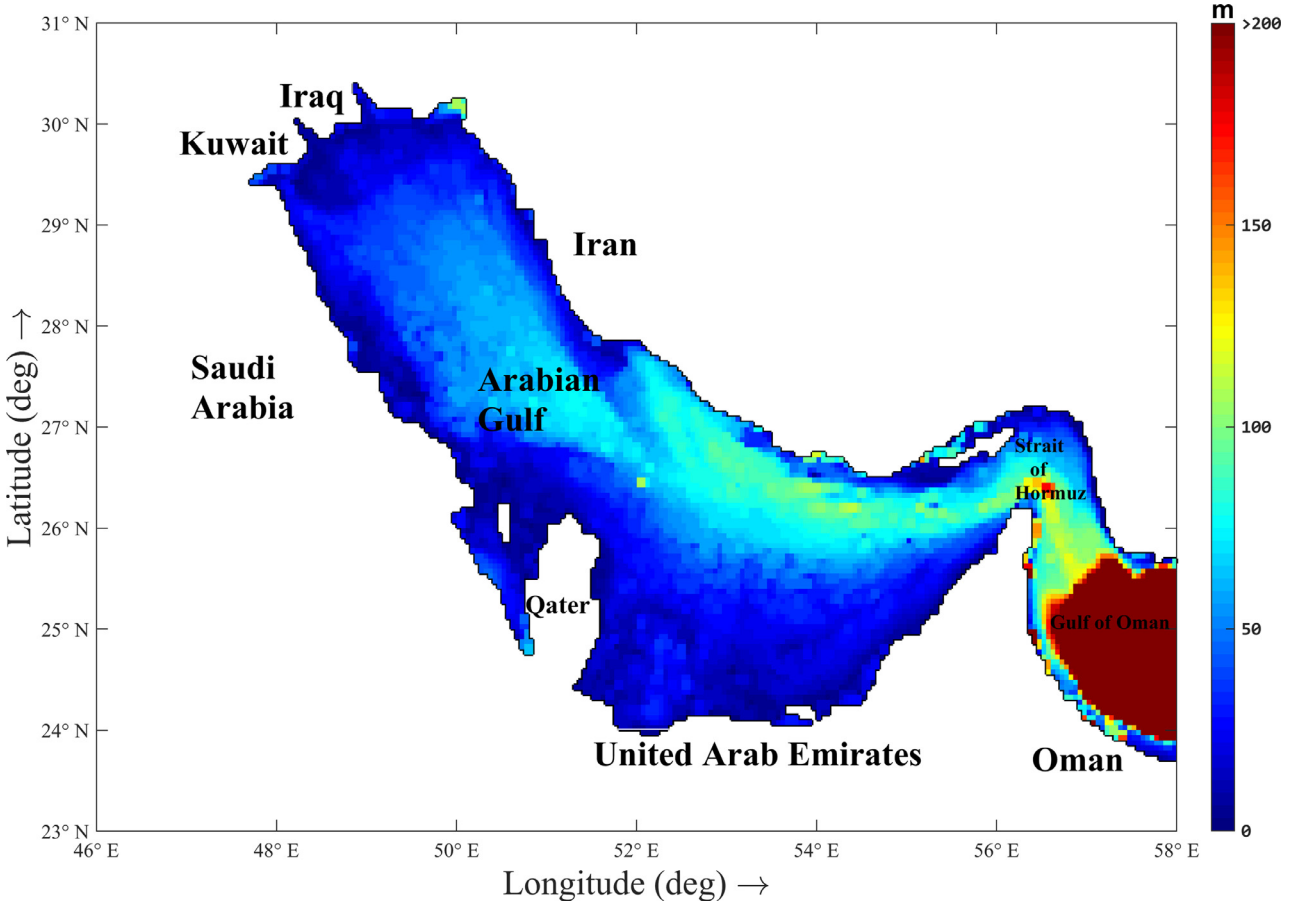

Figure 1 Map of the Arabian Gulf including numerical model bathymetry based on 'GEBCO_2021' global bathymetry datasets for the world ocean.

ern and one in the southern parts), and the latter forms only a single amphidromic point in the central part, near Bahrain. However, the earlier modelling studies showed that amplitudes and phases of the tidal components were not accurately produced by the used models, mainly due to using coarse mesh-resolution, as well as low resolution of bathymetry along the coastlines. Trepka (1968) used nonlinear Cartesian coordinate of Hansen Scheme to predict M_2 in the Gulf considering a coarse resolution grid (14 km). His model predictions of amplitude and phase were good in general, but large discrepancies of about 20% were found along the coastal areas. Later, he conducted an experiment considering 7 tidal constituents and compared the results with predictions of low and high water presented in the German and English Tide Tables. Their model discrepancies were in the range of 0.1 m in high and 0.36 m in low waters, with maximum deviation of about 60 min. Lardner et al. (1982) simulated the tides in the Gulf using the finite difference scheme considering a coarse grid (20 km) to generate the co-charts of the M_2 and K_1 constituents. They concluded that the computed amplitudes and phases are under-overestimated in several regions in the Gulf, due to the method of computation used, where the amplitudes are calculated as the average of all the maximum tidal elevations and the phases are calculated from the time of the last maximum of elevation. Later, Lardner et al. (1988) used the method of characteristics to predict M_2 and K_1 tidal constituents and compared their model results with co-tidal charts. They found that the phase contours are in good agreement while the amplitude contours include large discrepancies. They attributed the discrepancies to the low grid resolution along the coastline. Bashir (1993) modeled the tides using a $\sim$ 9 km grid model resolution and four tidal constituents (M_2, S_2, O_1, K_1) to drive the model. He validated his model using data from Admiralty chart, where his model tended to underestimate the amplitudes and overestimate the phases. Najafi and Noye (1997) modelled the AG tides using a Cartesian depth-averaged model and a spherical coordinate model (8.7 km x 9.7 km) forced by 10 tidal constituents mainly the major semidiurnal and diurnal and (L_2, μ_2). They found that the predicted phases for M_2 and O_1 are not consistent with the Admiralty charts in the strait of Hormuz. They attributed the discrepancies to the boundary effect. Pous et al. (2012) used a 9 km grid resolution model forced by 7 tidal constituents to generate only the co-charts for M_2 and K_1. They concluded that their model error ratio is in the order of 0.05 m (10%) on average with maximum discrepancies observed for P_1, O_1 and K_2. Recently, a modelling study by Poul et al. (2016) have considered 13 tidal constituents to describe the tides and focusing on effect of Qeshm canal in the Gulf, but only qualitative comparisons were provided in this study, thus, nothing can be stated about the discrepancies assessment.

As seen above that all previous modelling efforts used coarse-resolution models forced by a limited number of tidal constituents (depending on the study interest) along the open boundaries. In this study, we setup, calibrate and validate a vertically 2-D barotropic tidal model, considering a spatial horizontal mesh size of 5 km, bathymetry data at a resolution of 15 arc-seconds, and 13 tidal components along the open boundary. For this purpose, the *Delft3D* model, which was developed in the Netherlands by D*elft* Hydraulics is used. To select optimal parameters in the numerical model, sensitivity tests of the numerical and physical parameters were conducted. The simulation results were evaluated using water level measurements at 7 tide gauge stations and TOPEX/Poseidon (T/P) altimetry data. Moreover, one ADCP mooring station was used to validate the model in terms of U and V components. Once, the model has been validated, tidal conditions are described for the AG region. The rest of the manuscript is arranged as follows. Section 2 introduces the materials and methods, including a brief description of the modelling system and the AG Model configuration. The results and discussion of the numerical simulations are given in section 3. Section 4 sheds light on the summary and conclusion of this study.

2. Material and methods

2.1. Study area

The selected domain for the current study covers the entire AG basin including the Strait of Hormuz and part of the Gulf of Oman. The AG is located between 30°, 24°N latitude, and 48°, 57°E longitude, oriented in the NW and SE direction. It is a marginal, semi-enclosed hypersaline sea, with a maximum width of 370 km to a minimum of about 60 km found in the Strait of Hormuz. The length of the AG is about 1000 km along its main axis. The surface area of the water basin is about 239,000 km^2 (Emery, 1956). The bottom topography of the Gulf is relatively shallow, with a maximum depth of 90—100 m in the Strait of Hormuz, and a mean depth of about 35 m (Pous et al., 2004; Roos and Schuttelaars, 2011; Siddig et al., 2019). The deeper topographic features ($>$ 50 m) in the region are found along the Iranian coast while the shallower areas ($<$ 20 m) are found along the southwestern coasts. The AG is connected through the southern boundary with the Gulf of Oman (where the typical depth is $\sim$900 m), and the northern Indian Ocean via the Strait of Hormuz.

2.2. Data source

In this study, hourly time-series of tidal data at seven stations, namely Arabiyah Island, Jubail, Marjan Island, Qurayyah Pier, Ras Tanura, Mina Sulman, and Jask Harbour (see Figure 2 for their locations) were made available. These data were obtained from ARAMCO Oil Company except for Mina Sulman and Jask Harbour stations, they were downloaded from the Sea Level Centre at University of Hawaii (UHSLC) from the following link (http://uhslc.soest.hawaii.edu/data/?rq#uh182a). The hourly recorded time series from ARAMCO Oil Company covers the year 1999 while the sea level data for Mina Sulman and Jask Harbour includes the years 1997 and 2012 respectively. The main purpose of using the hourly tidal data is to carry out harmonic analysis and validate the numerical tidal model. Moreover, tidal constituents at 20 points selected within the model domain extracted from TOPEX/Poseidon (T/P) altimetry data (http://volkov.oce.orst.edu/tides/global) were considered to validate the numerical model. On the other hand, barotropic tidal currents in terms of U and V components

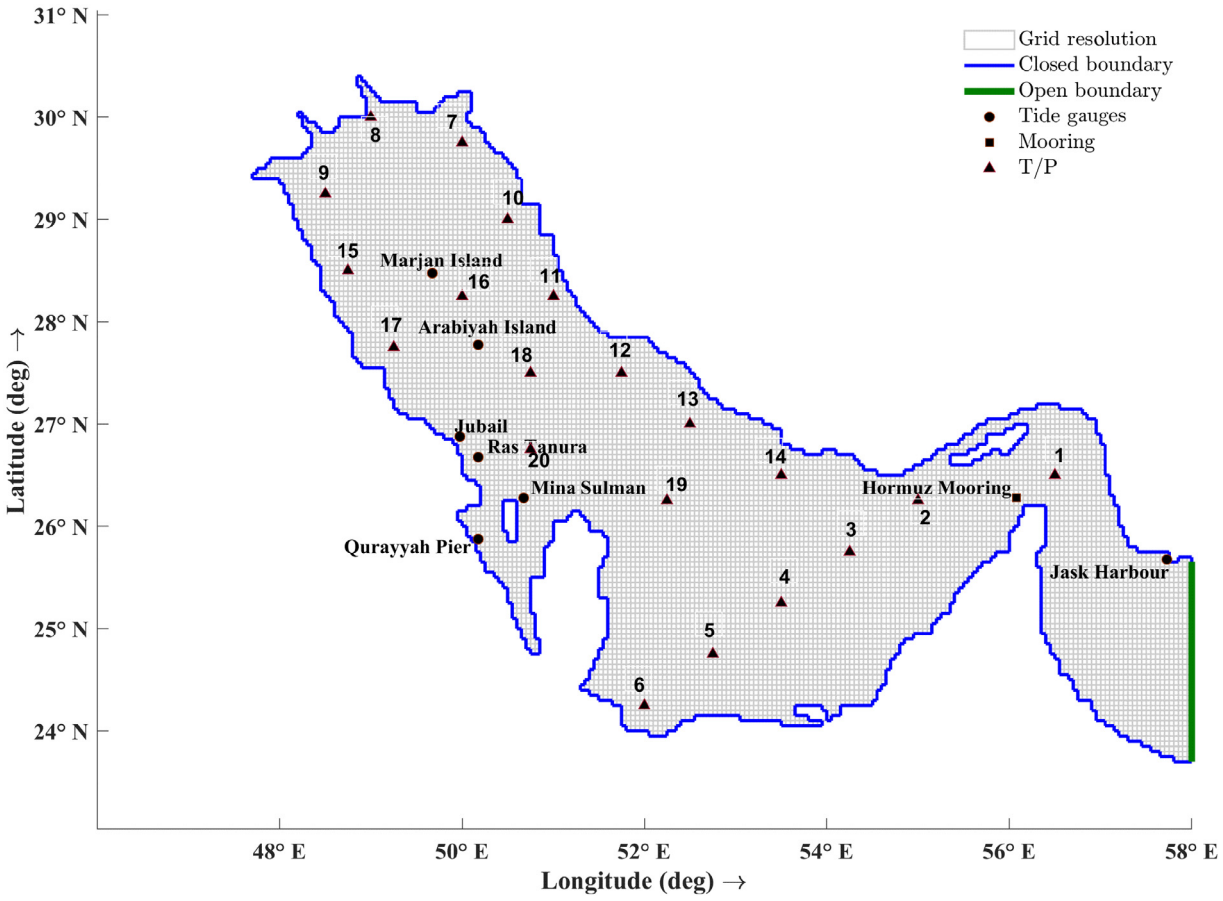

Figure 2 Computational grid distribution of the AG-Model, blue line represents the closed boundaries, green line represents the open boundary, (●) denotes tide gauge stations, and (■) denotes ADCP mooring, (▲) denotes T/P data locations.

(based on ADCP data) were taken from a published study (Johns et al., 2003) for the year 1997 at one station located in the Strait of Hormuz (26.2678°N, 56.0867°E) to validate the numerical model. The bathymetry data used is derived from the new release of the global bathymetry dataset "GEBCO_2021 Grid" at a 15 arc-second interval grid (~ 450 m), (https://www.gebco.net/data_and_products/gridded_bathymetry_data/gebco_2021/). To drive the tidal hydrodynamic model, 13 harmonic constituents, mainly semidiurnal tides (M_2, N_2, S_2, K_2) and diurnal tides (k_1, P_1, O_1, Q_1) including (M_f, M_m, M_4, MS_4, and MN_4) in the form of amplitudes and phases were extracted from the global ocean tidal model TPXO8 (Egbert and Erofeeva, 2002) (https://www.tpxo.net/global/tpxo8-atlas).

2.3. Statistical analysis

In the present study, several statistical parameters were considered to evaluate the performance of the numerical model. These are determined by calculating the *BIAS* (Eq. (1)), the index of agreement (*IOA*) (Eq. (2)), and the root mean square difference (*RMSD*) (Eq. (3)) based on the following formula:

$$BIAS = \frac{1}{n}\sum_{1}^{n} abs\,(Simulated - Observed) \tag{1}$$

$$IOA = \frac{\sum_{i=1}^{n}(O_i - S_i)^2}{\sum_{i=1}^{n}\left(|S_i - \bar{o}| + |O_i - \bar{o}|\right)^2},\ 0 \le IOA \le 1 \tag{2}$$

where o_i is the observation and s_i is the simulation and $\bar{o}$ is the average observation value (Willmott, 1981).

$$RMSD = \sqrt{\frac{1}{n}\sum_{1}^{n}(Simulated - Observed)^2} \tag{3}$$

On the other hand, the *Delft3D-TRIANA* program of the *Delft3D* modelling system has been employed to perform the tidal analysis and derive the main semidiurnal (N_2, M_2, S_2, K_2) and diurnals (Q_1, O_1, P_1, K_1) tidal constituents for both predictions and observations. The program also provides a statistical assessment of the discrepancies between observations and simulation results. The statistical assessment includes the standard deviation of the tidal analysis (SD), the Upper Extreme of the Residual (UER) and Lower Extreme of the Residual (LER), and the Summed Vector Difference (SVD) (Eq. (4)), which is calculated as:

$$\sum_{Obs}\sqrt{[H_C\cos(G_C) - H_O\cos(G_O)]^2 + [H_C\sin(G_C) - H_O\sin(G_O)]^2} \tag{4}$$

in which $\sum_{Obs}$ refers to a summation over the stations with observed amplitude and phase.

2.4. Model description

In the current research, the numerical hydrodynamic model was developed with the *Delft3D* modelling system. The modelling system was developed in the Netherlands by WL | D*elf*t Hydraulics (Deltares, 2011), The *Delft3D-Flow* model (the main module) is capable to solve two- (2D) or three-dimensional (3D) non-steady flow and transport processes produced from tidal and meteorological elements including the temperature and salinity differences effects. The *Delft3D* modelling system is based on the primitive Navier-Stokes equations for incompressible free surface flow, under the Boussinesq approximation (Roelvink and Banning, 1995). The system solves the momentum (Eq. (5)—(6), and continuity equations (Eq. (7)) for velocities and water levels. The equations include the horizontal equations of motion and the transport equations for conservative constituents.

The governing equations of the model are as follows:

$$\frac{\partial u}{\partial t}+u\frac{\partial u}{\partial x}+v\frac{\partial u}{\partial y}+g\frac{\partial \eta}{\partial x}-fv+\frac{gu|U|}{C^2\,(d+\eta)}-v_w\left(\frac{\partial^2 u}{\partial x^2}+\frac{\partial^2 v}{\partial y^2}\right)=0 \tag{5}$$

$$\frac{\partial v}{\partial t}+u\frac{\partial u}{\partial x}+v\frac{\partial v}{\partial y}+g\frac{\partial \eta}{\partial y}-fu+\frac{gv|U|}{C^2(d+\eta)}-v_w\left(\frac{\partial^2 u}{\partial x^2}+\frac{\partial^2 v}{\partial y^2}\right)=0 \tag{6}$$

$$\frac{\partial \eta}{\partial t}+\frac{\partial (d+\eta)u}{\partial x}+\frac{\partial (d+\eta)v}{\partial y}=0 \tag{7}$$

In which η is the water level elevation (m), d is the still water depth (m), f is the Coriolis parameter (1 s^{-1}), t is the time (s), U is the magnitude of the total velocity (m s^{-1}), C is the Chézy's friction coefficient ($m^{1/2}$ s^{-1}), u and v are the depth-averaged velocities in the x- and y-directions (m s^{-1}), v_w is the diffusion coefficient (m^2 s^{-1}), g is the acceleration due to gravity (m^2 s^{-1})

The numerical solution of the equations is discretized using the centred second-order finite differences method in a staggered Arakawa C-grid (Arakawa and Lamb, 1977). To solve the shallow water equations, the Alternating Differential Implicit (ADI) technique is used, which separates one integration time step into two stages. Therefore, the solution is implicit, and each stage is comprised of half a time step (Stelling and Leendertse, 1992). Since the solution is implicit, the consistency of the model is not limited by the time step. The wave propagation is primarily related to the Courant number (Eq. (8)), and to ensure accurate wave propagation in the grid, and accurate solution by Equation (8), the C_r is less than $4\sqrt{2}$ (Roelvink and Banning, 1995; Stelling and Leendertse, 1992).

$$C_r=2\Delta t\sqrt{gH\left(\frac{1}{\Delta x^2}+\frac{1}{\Delta y^2}\right)}<4\sqrt{2} \tag{8}$$

where C_r is the Courant number, Δt is the time step (s), g is the acceleration due to gravity (m s^{-2}), H is the local water depth (m), and Δx, Δy are the grid mesh sizes in the x- and y-directions (m).

2.5. Model configuration

The computational mesh of the AG model (hereafter AG-Model) covers the entire AG and extended to the Gulf of Oman at 58°E. The model area was structured using a rectangular grid with a uniform horizontal grid resolution of Δx and Δy =5 km (Figure 2). The figure also shows the positions of the water level observations considered in calibrating and validating the hydrodynamic model. The bathymetry of the AG-Model was based on the "GEBCO_2021 Grid" at a 15 arc-second interval grid ($\sim$ 450 m). The resulting bathymetric map based on this data is shown in Figure 1. In terms of open boundary, the modelling system (*Delft3D*) permits the use of the Riemann-invariant boundary condition to reduce error reflections in the open boundary (Verboom and Slob, 1984). When there is no incoming wave, then a zero Riemann invariant is imposed to ensure that all waves can leave the domain freely. The open boundary of the AG-Model was set at the Gulf of Oman (58°E). Along the open boundary, 13 harmonic constituents, mainly semidiurnal tides (M_2, N_2, S_2, K_2) and diurnal tides (K_1, P_1, O_1, Q_1) including (M_f, M_m, M_4, MS_4, and MN_4) in the form of amplitudes and phases were prescribed and linearly interpolated. The coordinates system of the AG-Model is spherical, which means that the variation of the Coriolis force is specified in the latitude direction. At the closed boundaries, a free slip condition was applied (U and V=0). In terms of initial conditions of water levels, they were set to zero. A time step of Δt = 60 seconds was set to carry out the simulations. The water density and gravitational acceleration values were set respectively 1028 kg m^{-3} and 9.81 m s^{-2}. The model was initialized for different periods, (1 January 1997, 1 January 1999, and 1 January 2012) and the simulations were carried out for 12 consecutive months. However, due to warming up processes, the equilibrium state was attained after ten days; thus, the first ten days of the simulation were removed before the analyses.

2.6. Tuning model parameters

Owing to the simplification, approximation, and assumptions employed in the numerical model, assessment of the model inputs is required (Palacio et al., 2005). To assess the general performance of the numerical model, sensitivity tests were carried out to adopt optimal numerical and physical parameters to the AG-Model. These parameters involved the boundary condition, time step, bottom roughness, and horizontal eddy viscosity (HEV). In terms of open boundary forcing, the model at eastern (U-direction) boundary was driven by the major eight semidiurnal and diurnal tidal components including (M_f, M_m, M_4, MS_4, and MN_4). The initial run showed that the AG-Model produces similar tidal elevations to the observed ones, therefore, the amplitudes and phases of the tidal components were adopted to carry out all simulations. On the other hand, changing the value of the time step did not influence the numerical model results; however, the smaller the time step, the higher the accuracy of the computations. As mentioned above that the wave propagation is related to the Courant number (Eq. (8)), accordingly, a time step of 1 minute was used in all runs to meet the stability criteria and accuracy requirements. The

Table 1 Sensitivity analysis of Chézy coefficient parameter.

Station ID	Water depth (m)	Chézy ($m^{1/2}$ s^{-1})	BIAS (m)	*RMSE* (m)	*IOA*
Arabiyah Island	56	45	0.06	0.19	0.97
		65	0.07	0.15	0.97
		85	0.07	0.13	0.97
Jubail	10	45	0.07	0.26	0.98
		65	0.07	0.19	0.98
		85	0.08	0.14	0.98
Marjan Island	46	45	0.07	0.17	0.94
		65	0.08	0.14	0.94
		85	0.08	0.12	0.95
Qurayyah Pier	25	45	0.08	0.10	0.75
		65	0.06	0.08	0.85
		85	0.03	0.04	0.95
Ras Tanura	8	45	0.10	0.29	0.98
		65	0.10	0.23	0.98
		85	0.10	0.22	0.98
Mina Sulman	11	45	0.01	0.32	0.99
		65	0.01	0.25	0.99
		85	0.01	0.23	0.99
Jask Harbour	10	45	0.01	0.07	0.99
		65	0.01	0.07	0.99
		85	0.01	0.07	0.99

Note: The P-value related to all comparisons is very low (P > 0.0001), indicating that the results from correlation are significant. *IOA* represents Index of agreement; *RMSD* represents Root mean square difference and BIAS.

Delft3D model applies Chézy coefficient formulation ($c=\frac{H^{1/6}}{n}$) which is based mainly on the bottom roughness and the water depth height. The bottom roughness is an important parameter that plays a crucial role in the hydrodynamic flow models. To investigate its influence on the model results, three different Chézy coefficient values of 45, 65, and 85 $m^{1/2}$ s^{-1} as uniform over the entire domain were examined (Table 1). The analysis revealed that using higher or lower values from 65 $m^{1/2}$ s^{-1} (a default value of the *Delft3D* system) causes slight influences on the model results. However, the simulations carried out with bottom roughness (Chézy) of 85 $m^{1/2}$ s^{-1} led to provide better results based on the values of *RMS* error. Therefore, a constant Chézy bottom-roughness coefficient of 85 $m^{1/2}$ s^{-1} was applied temporally and spatially throughout the model domain. Owing to its essential role in defining turbulence mixing, the influence of the HEV was also tested by comparing different cases with the original simulation. It was found that the EHV coefficient has insignificant influence on the outcome of the simulation. The optimal settings chosen for the final simulations of the AG tidal hydrodynamics are summarized in Table 2.

Table 2 Numerical and physical parameters adopted for the AG-Model.

Parameters	Value	Unit
Grid Resolution	5	(km)
Time Step	60	(s)
Chezy Coefficient	85	($m^{1/2}$ s^{-1})
Horizontal Eddy Viscosity (HEV)	1	(m^2 s^{-1})
Water Density	1028	(kg m^{-3})
Gravitational Acceleration	9.81	(m s^{-2})

3. Results and discussion

A 2-D hydrodynamic tidal model (5 km) has been setup for the entire AG system environment to study the tidal characteristics. To test the performance and quality of the AG-Model settings, two approaches were considered. Firstly, the model performance was assessed by comparing the model results in terms of water level with available hourly observed time series and tidal constituents based on T/P data. The model performance was also assessed by comparing the model results in terms of current velocities (U and V components) with the previous observational study of (Johns et al., 2003) for the year 1997. Both qualitative and statistical comparisons were carried out. In the second approach, discrepancies in terms of amplitudes and phases for the major semidiurnal and diurnal astronomical components were quantified statistically. In the following, the model evaluation, co-charts analysis, and simulated tidal currents are discussed.

3.1. Tidal elevation

In this section, comparisons of tidal elevations and statistical assessments of discrepancies between the model simulations and observations are presented. Figure 3a–g shows examples of the qualitative comparison for all stations, while Table 3 lists the statistical assessment. In general, the figure shows a good match between the simulated and observed

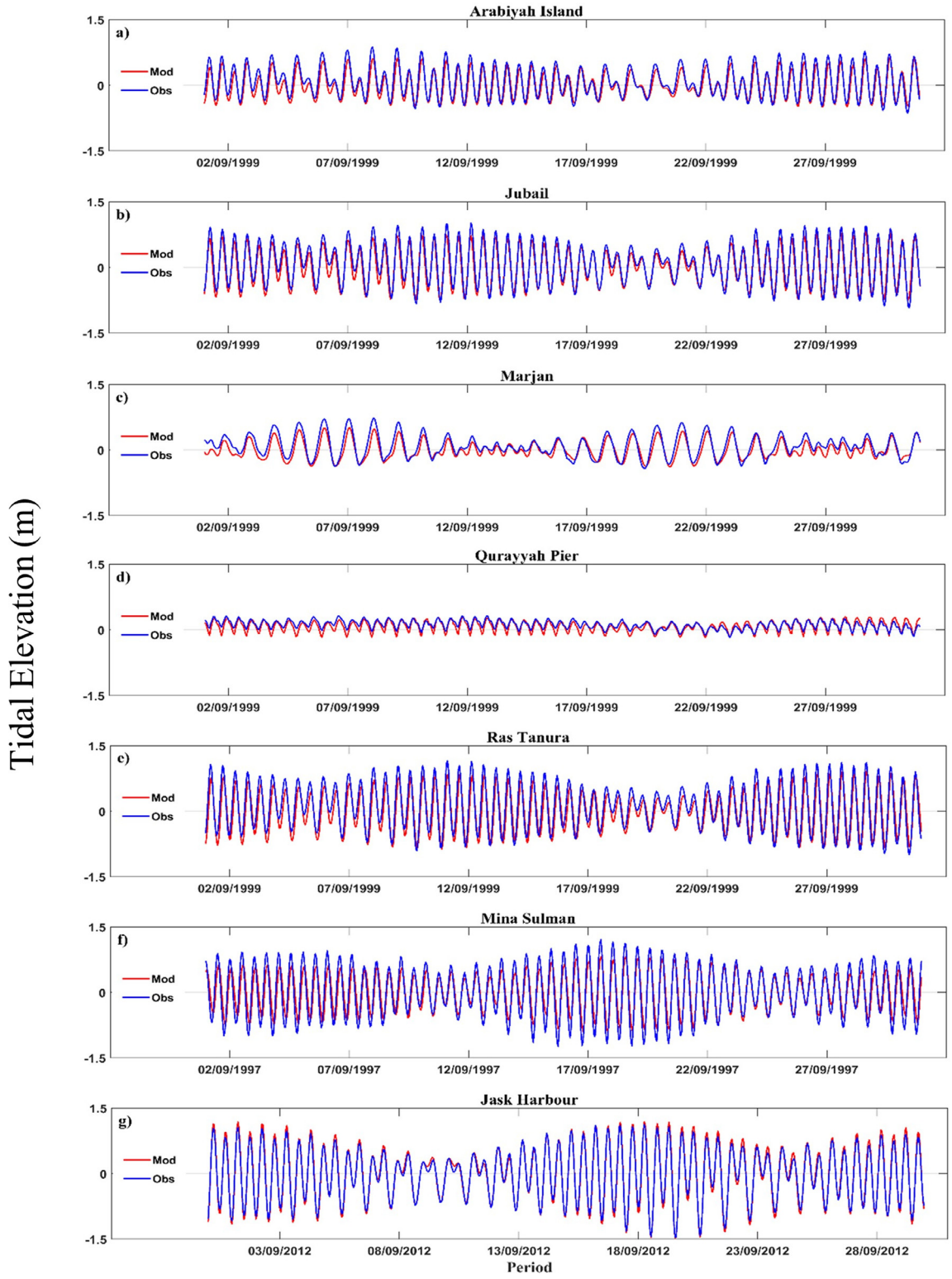

Figure 3 Comparisons between tidal predictions and observations at (a) Arabiyah Island, (b) Jubail, (c) Marjan, (d) Qurayyah Pier, (e) Ras Tanura, (f) Mina Sulman, (g) Jask Harbour.

tidal elevations. This is confirmed by predicting low and high water during neap and spring tidal cycles (Figure 3) and by reproducing the different tidal regimes in the Gulf region. However, there is an underestimation of high/low water at all stations, except for Jask Harbour. It is pronounced largely at Ras Tanura and Mina Sulman stations. These discrepancies may arise from several aspects, the most important is the bathymetry of the model, especially the

Table 3 Statistical analysis of all stations considered in the model validation.

Station No.	Station ID	*BIAS* (m)	*RMSD* (m)	*IOA*
1	*Arabiyah Island*	0.07	0.13	0.98
2	*Jubail*	0.08	0.14	0.99
3	*Marjan Island*	0.08	0.12	0.95
4	*Qurayyah Pier*	0.03	0.04	0.96
5	*Ras Tanura*	0.10	0.22	0.98
6	*Mina Salman*	0.01	0.23	0.99
7	*Jask Harbour*	0.01	0.07	0.99

Note: The P-value related to all comparisons is very low ($P > 0.0001$), indicating that the results from correlation are significant. *IOA* represents Index of agreement; *RMSD* represents root mean square difference and BIAS.

shallow coastal bathymetry. Previous studies indicated that the performance and accuracy of tidal regional models depend highly on correct seabed data, where these models are often restricted by seabed data, especially in shallow regions (Madah et al., 2015; Quaresma and Pichon, 2013). Moreover, the locations of the tide gauge stations of Ras Tanura and Mina Sulman are mainly at port constructions or marine platforms, which have topographic influences. Such influences may be difficult to be resolved by the present numerical model because of the mesh resolution and bathymetry along these locations. This suggests that using high-resolution bathymetry data in shallow regions is indispensable for tidal simulation in the AG. For phase conditions, there is a very slight phase lag between the model simulations and observations, pronounced mainly at the Marjan station (Figure 3).

To further quantify the discrepancies between the water level observations and the AG-Model predictions, calculation of the respective discrepancies at the high/low water level was conducted (Table 3). Statistical parameters have been determined for each observation point considered in the visual interpretation for Figure 3. In general, Table 3 shows a very good agreement between the water level observations and simulated time series. It was found that *RMS* error ranges from 0.07 to 0.23 m while the *BIAS* value varies from 0.01 to 0.1 m with maximum discrepancies observed at Ras Tanura and Mina Sulman stations. However, the *IOA* between the simulated and observed water levels was significant with p-values less than 0.0001. The *IOA* values are found to be varied between 0.95—0.99 for all stations. These statistical values reflect that the AG-Model is able to reproduce the tidal levels in the Arabian Gulf region to a very good degree.

Further validation of the AG-Model was carried out considering T/P altimetry data at 20 points selected within the Gulf domain (see Figure 2 for their locations). In general, the predicted amplitudes and phases of semidiurnal and diurnal tidal constituents are in very good agreement with the values of T/P data (Figure 4a, b).

In the second approach, harmonic analysis of the simulated and observed tidal data was performed to evaluate the discrepancies in terms of amplitude and phase of the major semidiurnal and diurnal astronomical components. An overview of the discrepancies at the stations of Jask Harbour, Qurayyah, Ras Tanura, and Marjan Island is presented in Table 4. The last column in the table lists the signal-to-noise ratio (*SNR*). The results of the other stations are shown in Appendix A. Statistical assessment of the discrepancies which includes *SD*, *UER*, *LER*, and *SVD* of the residuals based on the *Delft3D-TRIANA* tool is presented in Table 5.

From Table 4, the simulated and observed amplitudes errors ($H_C - H_O$) of all components are found to be in the range of a few centimetres, varying between -0.065 to 0.02 m in all stations. Maximum discrepancies are found for the M_2 tidal wave in the Marjan and Ras Tanura stations (0.020 and -0.055) respectively and K_1 tidal wave (-0.065) in the Marjan station only. However, the Mina Sulman station having slightly the largest discrepancies as shown in Appendix A. Excluding this station, the results indicate that the tidal model (AG-Model) in terms of amplitudes of the major semidiurnal and diurnal tides is performing well. On the other hand, the amplitude ratio (H_c / H_o) for semidiurnal tidal constituents is found to be 1 in all stations except the Marjan station, which is showing a slightly larger value, while for diurnal constituents is ranged between 0.5 to 1. The phase errors ($G_c - G_o$) between the computed and observed tidal constituents are observed to be satisfactorily in all stations, with maximum phase errors observed at Ras Tanura station for S_2. Statistical assessment in Table 5 shows that the *SD* of the tidal analysis is close to zero. In terms of *LER* and *UER*, they range from -0.13 to -0.09, and from 0.03 to 0.16, respectively. The *SVD*, (which is a ratio for the total discrepancies of all constituents) is found to be 0.074, 0.269, 1.397, and 0.741 for Jask Harbour, Qurayyah, Ras Tanura, and Marjan Island stations, respectively. These results indicate that the tidal model (AG-Model) in terms of amplitude and phase is performing well.

3.2. Co-amplitude and co-phase charts analysis

To generate co-tidal charts, the tidal components obtained from the harmonic analysis of the AG-Model outcomes were used. Three dominant tidal regimes have been identified in the AG, mainly the mixed, semidiurnal, and diurnal tides (e.g., Akbari et al., 2016; Siddig et al., 2019). As mentioned in the introduction that previous modelling studies considered only the four tidal components (M_2, S_2, P_1, O_1) to show co-amplitude and co-phase charts. In this study, the four major tidal constituents of each tidal regime (M_2, N_2, S_2, K_2, K_1, P_1, O_1, Q_1) dominate the region were considered in the analysis to enhance our understanding and knowledge of the tidal hydrodynamics in the AG. The resulting co-amplitudes and co-phases were analysed and compared with the previous modelling studies as well as the British

Table 4 Comparison between amplitudes and phases of computed and observed tidal components for Jask Harbour, Qurayyah Pier, Ras Tanura, and Marjan stations.

Components	*Jask Habour*								*Qurayyah Pier*							
	H_o	H_c	G_o	G_c	$H_c - H_o$	$G_c - G_o$	H_c / H_o	*SNR*	H_o	H_c	G_o	G_c	$H_c - H_o$	$G_c - G_o$	H_c / H_o	*SNR*
M_2	0.681	0.666	155.7	156.9	0.015	1.2	1.02	6E+04	0.08	0.095	252.5	195.0	0.011	-57.7	1.10	4E+04
S_2	0.265	0.259	185.0	187.9	0.006	3.0	1.02	8E+03	0.02	0.024	309.9	238.0	0.002	-71.7	1.10	2E+03
N_2	0.166	0.166	140.9	139.7	0.000	-1.2	1.00	3E+03	0.02	0.018	219.5	161.0	0.003	-58.4	1.20	1E+03
K_2	0.076	0.069	180.6	182.3	0.007	1.7	1.10	5E+02	0.01	0.007	289.0	229.0	0.000	-60.4	1.00	2E+02
K_1	0.395	0.397	338.4	339.8	-0.002	1.4	1.00	9E+03	0.03	0.017	110.3	48.5	-0.008	-61.8	0.70	2E+03
O_1	0.205	0.205	339.6	341.8	0.000	2.2	1.00	3E+03	0.02	0.014	24.5	348.0	-0.003	-36.9	0.80	1E+03
P_1	0.117	0.122	335.2	338.5	-0.005	3.3	0.96	1E+03	0.01	0.003	83.5	13.6	-0.003	-69.9	0.50	8E+01
Q_1	0.044	0.045	345.4	344.5	-0.001	-0.9	0.97	1E+02	0.00	0.002	6.6	309.0	0.000	-57.6	1.00	2E+01
Components	*Ras Tanura*								*Marjan*							
	H_o	H_c	G_o	G_c	$H_c - H_o$	$G_c - G_o$	H_c / H_o	*SNR*	H_o	H_c	G_o	G_c	$H_c - H_o$	$G_c - G_o$	H_c / H_o	*SNR*
M_2	0.613	0.558	128.9	63.0	-0.055	-65.9	0.91	6E+04	0.056	0.076	262.8	204.0	0.020	-59.0	1.36	4E+03
S_2	0.216	0.179	185.2	111.8	-0.037	-73.4	0.82	8E+03	0.031	0.035	216.8	165.0	0.004	-51.7	1.14	1E+03
N_2	0.125	0.118	98.8	30.1	-0.007	-68.7	0.94	3E+03	0.015	0.018	155.7	92.0	0.004	-64.2	1.25	3E+02
K_2	0.080	0.075	177.2	104.4	-0.005	-72.9	0.90	5E+02	0.008	0.010	17.5	324.0	0.003	-53.5	1.25	6E+01
K_1	0.147	0.120	339.1	298.2	-0.027	-40.9	0.81	9E+03	0.312	0.248	97.2	67.0	-0.065	-29.9	0.80	3E+03
O_1	0.116	0.104	281.2	254.4	-0.012	-26.8	0.90	3E+03	0.193	0.169	137.1	119.0	-0.024	-18.3	0.90	1E+03
P_1	0.045	0.032	328.4	283.0	-0.013	-45.4	0.70	1E+03	0.097	0.072	101.8	70.0	-0.025	-31.6	0.74	3E+02
Q_1	0.020	0.020	269.8	230.1	0.000	-39.7	0.98	1E+02	0.033	0.030	23.3	0.3	-0.003	-23.0	0.91	3E+01

H_o: amplitude of observed tide, ***G_o***: phase of the observed tide, ***H_c***: amplitude of simulated tide, ***G_c***: phase of the simulated tide, ***H_c - H_o***: amplitude difference, ***G_c - G_o***: Phase difference, ***H_c / H_o***: Amplitude ratio, ***SNR***: signal-to-noise ratio.

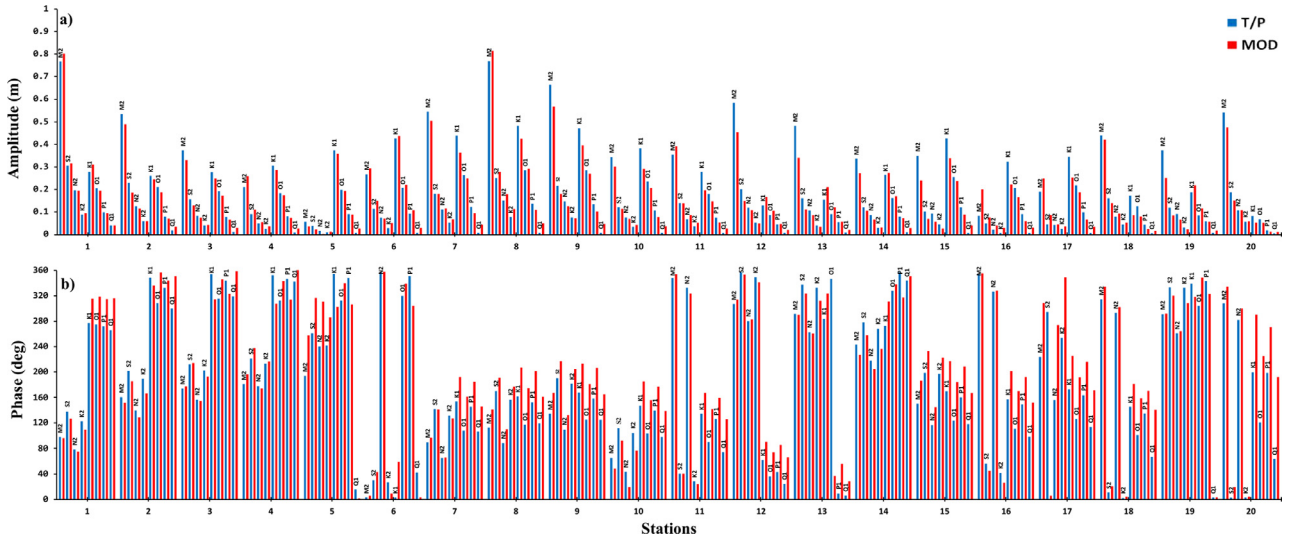

Figure 4 Comparisons of tidal (a) amplitudes and (b) phases between the AG-Model and T/P data.

Table 5 Statistical Assessment obtained from *Delft3D-TRIANA*.

Parameters	Station ID			
	Jask Harbour	*Qurayyah Pier*	*Ras Tanura*	*Marjan Island*
SD	0.008	0.029	0.047	0.030
LER	-0.027	-0.090	-0.130	-0.103
UER	0.032	0.092	0.165	0.091
SVD	0.074	0.269	1.397	0.741

SD: Standard deviation of tidal Analysis; **LER:** Lower extreme for residuals; **UER:** Upper extreme for residuals; **SVD:** Summed vector differences.

Admiralty (Admiralty, 2012) co-charts especially, the M_2, S_2, K_1, and O_1 tidal constituents.

3.2.1. Semidiurnal constituents

Co-amplitudes and co-phases of the major semidiurnal constituents (M_2, S_2, N_2, K_2) are displayed in Figure 5a–d, respectively. In general, the amplitudes of M_2, S_2, N_2, and K_2 tidal waves have the same performance in the AG basin. The dominant pattern of these tidal waves is the generation of two anticlockwise amphidromic points, one is in the northwestern part, and one is in the southern end of the basin centred around 28.25° and 24.5°N, respectively.

The M_2 tidal wave represents the largest among other constituents with a maximum amplitude of 0.9 m. The amplitude of S_2 tidal wave is low and represents almost 30% of the M_2, while N_2 and K_2 tides are relatively smaller in amplitudes compared to the S_2 tide. As can be seen from the figure that the semidiurnal M_2, S_2, N_2, and K_2 tidal waves have amplification in tidal height at several locations inside the AG basin (Figure 5). These locations are, the northern end of the Gulf (near Kuwait, Iraqi coast, and the northern coast of Iran), the middle part of the basin, mainly on the eastern coast (Iran) and on the Saudi coast, the northern Bahrain, the southwestern end of the basin and the Strait of Hormuz. On the other hand, the co-amplitude chart shows low amplitudes at the southeast coast of Iran, the UAE coast, the eastern coast of Qatar, the south of Bahrain, the Saudi coast, mainly in the vicinity of the Ras Tanura, Qurayyah Pier, and Mina Sulman stations. Figure 5 also shows the calculated phases for the major semidiurnal tidal constituents in the AG. In general, the tidal amplitudes and phases are in good agreement with the co-amplitude and co-phase lines of the British Admiralty charts (Admiralty, 2012).

3.2.2. Diurnal constituents

co-amplitudes and co-phases of the major diurnal constituents (K_1, P_1, O_1, Q_1) are shown respectively in Figure 6a–d, respectively. The major feature of these tidal waves is the generation of a single amphidromic point in the central portion of the AG centred around 26.8°N (North Bahrain). In general, the diurnal constituents show amplification in tidal amplitude at several different locations, with a minimum value in the central part where a virtual amphidromic system is developed.

The diurnal component K_1 represents the largest among other constituents with a maximum amplitude of 0.42 m. The amplitude of O_1 tidal wave is about 50% lower than the K_1 tide, while P_1 and Q_1 tides are smaller in amplitudes compared to the O_1 tide. Maximum computed amplitudes for P_1 and Q_1 are respectively 0.1 and 0.04 m (Figure 6 c, d). The K_1, P_1, O_1, and Q_1 tidal waves have amplification in tidal height toward the head of the Gulf (Kuwait, Iraqi coasts, and northern coast of Iran), and the southeastern coast of Qatar, the southern Emirate coast, and

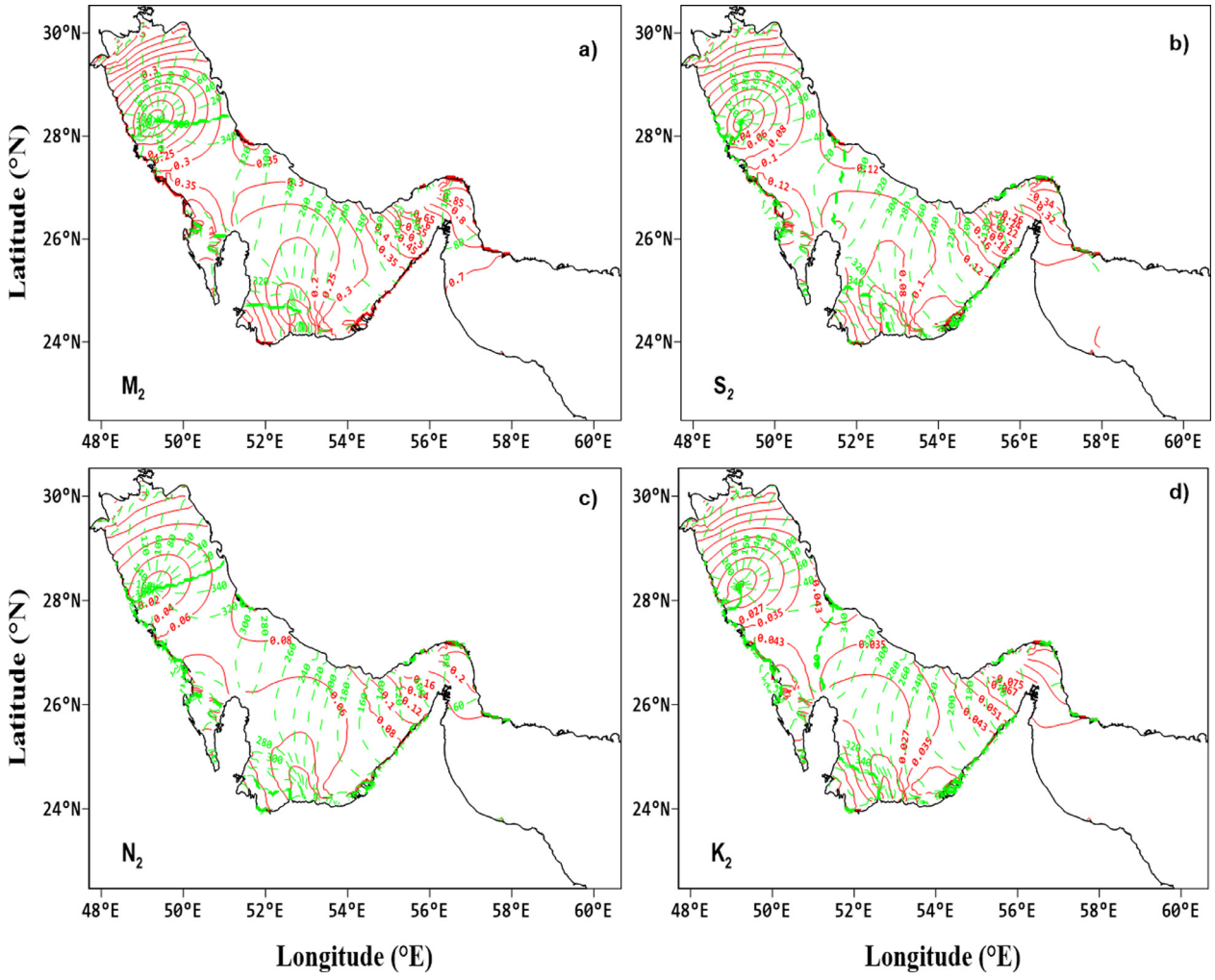

Figure 5 Co-amplitudes (red solid-lines) and co-phases (green dashed-lines) of major semidiurnal components (M_2, S_2, N_2, K_2).

the Gulf of Oman including the strait of Hormuz (Figure 6). The patterns observed along the southern Emirate coast are consistent with the tidal values reported in the coastal studies by Balaji (2012) and Mohamed and El-Dahshan (2002), however, they were not shown in the previous modelling studies. On the other hand, low amplitudes were observed at the south of Bahrain, the Saudi coast (mainly in the vicinity of Qurayyah Pier and Mina Sulman stations), the UAE coast, the south-western coast of Qatar. The computed amplitudes and phases are in good agreement with the British Admiralty Charts (Admiralty, 2012).

The above basic tidal patterns, in general, are consistent with all previous modelling studies and the British Admiralty charts (Admiralty, 2012); however, the position of the amphidromic points especially for semidiurnal constituents as well as locations of high/low amplitudes are slightly different when comparing with some previous modelling studies but comparable to the latter. The Admiralty (2012) charts, Lardner et al. (1988, 1982), Trepka (1968), Najafi and Noye (1997), and our model results show that the position of the amphidromic systems produced by (M_2, S_2) tidal waves is close to the western coast, unlike few studies that showed positions that are mostly near the centre of the basin. However, Lardner et al. (1982) produced the co-chart for M_2 with under- overestimation in some areas and later produced the amplitudes and phases of M_2 and K_1 tidal waves with also underestimations of amplitudes due to the coarse grid model used along the coastline (20 km) (Lardner et al., 1988). Moreover, Trepka (1968) found that the amplitude error of S_2, K_1, and O_1 tidal constituents was large. He recommended using a finer grid resolution and more than 7 tidal constituents along the open boundary to get the prediction of the minor tides. Najafi and Noye (1997) also modelled the AG tides using Cartesian coordinates to produce the M_2, S_2, K_1, and O_1 tidal charts and found that the predicted phases were not well reproduced by the model.

3.3. Sensitivity analysis for the number of tidal constituents at the open boundary

To test the accuracy of the numerical model in representation of the tidal conditions in the Gulf region, three different scenarios were carried out considering different number of tidal constituents along the open boundary. In the first scenario (SN-1), the model was run using only the four tidal constituents (M_2, S_2, K_1, O_1) at the open sea boundary. In the second scenario (SN-2), the model was driven

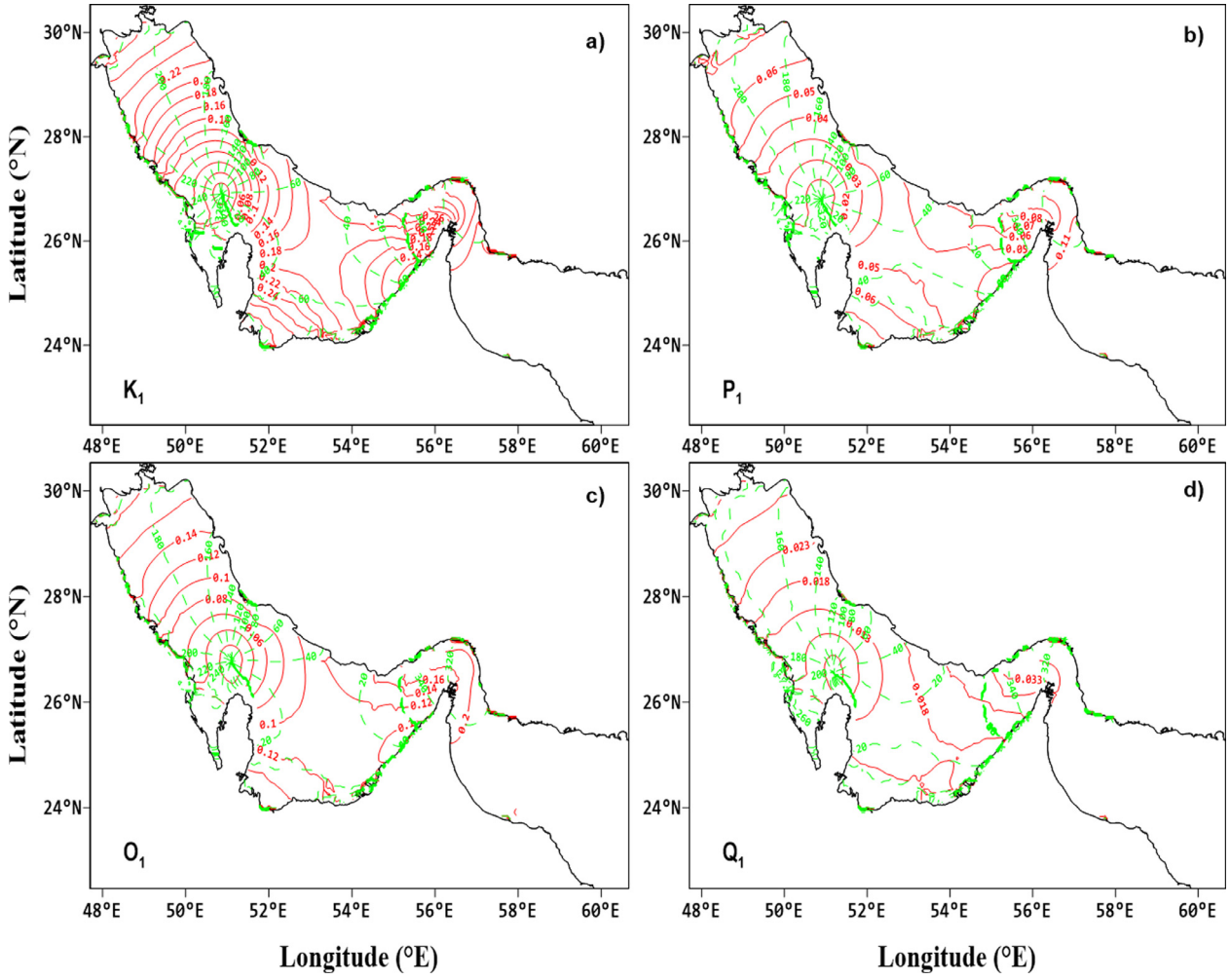

Figure 6 Co-Amplitudes (red solid-lines) and co-phases (green dashed-lines) of major diurnal components (K_1, P_1, O_1, Q_1).

by the major eight semidiurnal (M_2, N_2, S_2, K_2) and diurnal tidal components (K_1, O_1, P_1, Q_1). In the third scenario (SN-3), the same as the second one but with additional five tidal constituents (M_f, M_m, M_4, MS_4, MN_4). Figure 7 shows an example of the model predictions of the three scenarios against the observations at two coastal stations (Ras Tanura and Mina Sulman), while Table 6 lists the statistical assessment for all stations considered in the analysis. The initial simulation (SN-1) shows that the AG-Model produces similar tidal elevations to the observed ones, however the discrepancies are large at the coastal areas, where the *RMSE* varies between 0.12 to 0.28 m. The simulation of the SN-2 shows slight improvements in tidal amplitudes compared with the SN-1. The *RMS* error ranges from 0.07 to 0.25 m with maximum discrepancies found at the coastal stations (Ras Tanura and Mina Sulman). The tidal predictions of the last scenario (SN-3) confirms that the AG-Model produces better results compared to the two previous scenarios (SN-1 and SN-2), especially at the coastal stations, where the discrepancies are less than 0.24 m (Figure 7 and Table 6).

The statistical assessment in Tables 3 and 5 also confirms the model ability to reproduce the tidal regimes in the Gulf accurately. This indicates that using 13 tidal constituents along the open boundary is very important in simulating the tidal conditions in the AG region. Such tidal constituents are necessary to be incorporated to reproduce the regional propagation of tidal waves (Quaresma and Pichon, 2013), thus, they can interact nonlinearly. The AG-Model predictions based on using 13 tidal constituents along the open boundary conditions showed a very good agreement with the water level time series observations in the Gulf region (Figure 3). Maximum discrepancies in amplitudes are found in the range of 0.065 m at Marjan station only for K_1, while on average, the errors for all tidal constituents considered in the analysis are in the order of less than 0.02 m (4%) (Table 4 and Appendix A). This error value is reflecting a very good performance of the AG-Model compared with the previous modelling studies carried out in the Gulf, where minimum discrepancies (on average 0.05 m, 10%) were found in the study by Pous et al. (2012) who used only 7 tidal constituents along the open boundary. On the other hand, the comparison of the tidal constituents between the AG-Model and T/P altimetry data showed a very good agreement (Figure 4), indicating the effectiveness of the tidal constituents prescribed along the open boundary in explaining the tidal conditions in the Gulf region.

Although the AG-Model underestimates slightly the amplitudes of the tidal constituents, especially at Ras Tanura,

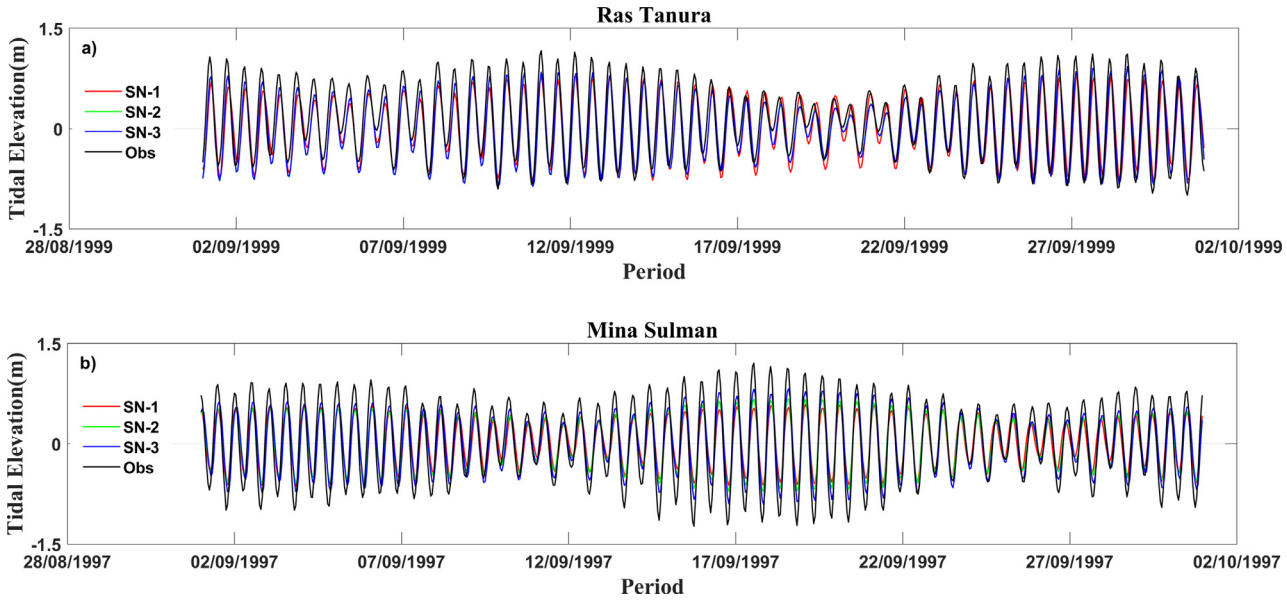

Figure 7 Comparisons between tidal predictions and observations at (a) Ras Tanura and (b) Mina Sulman stations considering a different number of tidal constituents at the open boundary.

Table 6 Statistical analysis for the number of tidal constituents at the open boundary.

Station ID	*Scenarios*	*RMSE (m)*
Arabiyah	SN-1: 4TC	0.15
Island	SN-2: 8TC	0.14
	SN-3: 13TC	0.13
Jubail	SN-1: 4TC	0.16
	SN-2: 8TC	0.15
	SN-3: 13TC	0.14
Marjan	SN-1: 4TC	0.12
Island	SN-2: 8TC	0.13
	SN-3: 13TC	0.12
Qurayyah	SN-1: 4TC	0.08
Pier	SN-2: 8TC	0.07
	SN-3: 13TC	0.04
Ras	SN-1: 4TC	0.26
Tanura	SN-2: 8TC	0.23
	SN-3: 13TC	0.22
Mina	SN-1: 4TC	0.28
Sulman	SN-2: 8TC	0.25
	SN-3: 13TC	0.23
Jask	SN-1: 4TC	0.17
Harbour	SN-2: 8TC	0.08
	SN-3: 13TC	0.07

Note: The **TC** represents tidal constituents, ***RMSE*** represents Root mean square difference. SN-1: [M_2, S_2, K_1, O_1]; SN-2: [M_2, S_2, N_2, K_2, K_1, O_1, P_1, Q_1]; SN-3: [M_2, S_2, N_2, K_2, K_1, O_1, P_1, Q_1, M_f, M_m, M_4, MS_4, MN_4]

Mina Sulman stations (the western coast) as shown from the statistical analysis (Section 2.3), the model captures all regions of high and low amplitudes accurately (Figure 5, 6) identical to the British Admiralty Charts (Admiralty, 2012). However, the coastal areas of Ras Tanura and Mina Sulman stations are shallow and complex due to coastal constructures, indicating that the grid resolution along these stations is inadequate to resolve the tidal amplitudes accurately. These results may be improved by applying a nesting approach as explained by Spall and Holland (1991), considering parent and child grids with changing grid spacings, in which the child grid has a finer resolution in areas of question. In this approach, the data is exchanged between the coarse parent grid and the finer child grid, allowing the child model to resolve better the tidal hydrodynamic patterns in such complex regions, as applied in several regional ocean modelling (e.g., Barth et al., 2005; Debreu et al., 2012; Mason et al., 2010). In this frame, the numerical model reliability would be enhanced, thus, the AG-Model can be applied as a regional model.

3.3. Form factor analysis

To find out the relative importance of the semidiurnal and diurnal tidal components in the AG, the form factor (*FF*) is calculated based on (Pugh, 2004):

$$FF = \frac{O_1 + K_1}{M_2 + S_2}$$

where O_1, K_1, M_2, and S_2 are the elevation amplitudes of the indicated components. To classify, if $FF < 0.25$ the tide is semidiurnal; if *FF* is between 0.25 and 1.5, the tide is mixed semidiurnal; if *FF* is between 1.5 and 3, the tide is mixed diurnal, and when $FF > 3$, the tide is diurnal. Figure 8 shows the spatial distribution of the *FF* in the AG basin. As can be observed that the AG-Model reproduces the tidal types observed in the region accurately, where the tidal type varies according to the location. The relative importance is clear in the northern and southern portions of the AG where anticlockwise amphidromic points are developed, and it is not constant in the whole AG. Thus, the diurnal tide is greater in the northern and southern parts of the AG, showing mixed

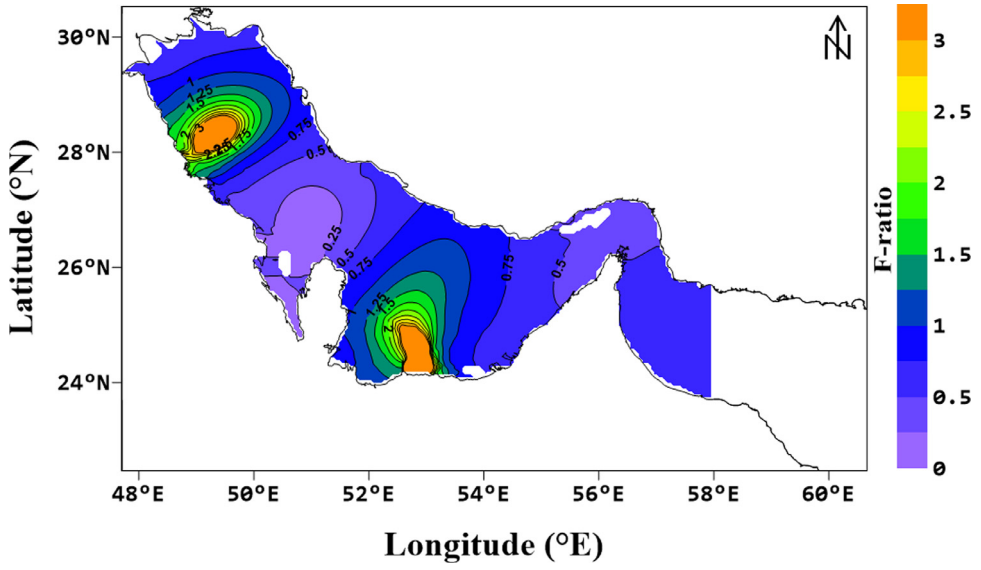

Figure 8 Distribution of form factor based on the model results.

Table 7 Comparison between amplitudes and phases of computed and observed tidal components of East velocities (m s^{-1}) at the Strait of Hormuz for the year 1997.

Components	H_o	H_c	G_o	G_c	$H_c - H_o$	$G_c - G_o$	H_c / H_o
M_2	0.208	0.249	35.4	42.0	0.041	6.7	1.1
S_2	0.085	0.096	69.3	74.1	0.011	4.8	1.1
N_2	0.053	0.059	18.2	24.6	0.006	6.4	1.1
K_1	0.236	0.228	204.6	213.8	-0.008	9.1	0.9
O_1	0.091	0.107	177.5	202.0	0.016	24.6	1.1
P_1	0.072	0.063	185.9	210.5	-0.009	24.6	0.9

H_o: amplitude of observed tide, G_o: phase of the observed tide, H_c: amplitude of simulated tide, G_c: phase of the simulated tide, H_c - H_o: amplitude difference, G_c - G_o: Phase difference, H_c / H_o: Amplitude ratio.

nature dominant with semidiurnal and diurnal components on the eastern coast and the western coast respectively. The figure reveals that the diurnal nature (orange) dominates in the northern part of the AG, at around 28°N; while the surrounding is dominated by the mixed tides, mainly diurnal (green) and semidiurnal (blue). Similar characteristics are observed in the southwestern part of the basin, at approximately 24.5°N, while the central part of the AG and the strait of Hormuz are dominated by semidiurnal components (purple). These results agree with the previous studies in the region (e.g., Akbari et al., 2016; Siddig et al., 2019).

3.4. Tidal currents

To evaluate the simulation results in terms of U and V components, barotropic tidal currents based on ADCP observations reported in Johns et al. (2003) for the year 1997 at one station located in the Strait of Hormuz were considered. Table 7,8 list the comparisons between amplitudes and phases of observed and simulated tidal constituents of east and north velocities, while Table 9 shows the statistical assessment. The comparison indicates that the simulated and observed amplitude errors ($H_C - H_O$) of M_2, N_2, S_2, K_1, P_1, and O_1 are found to be in the range of a few m s^{-1}, varying between -0.01 to 0.041 m s^{-1} for east and north velocity components. The maximum discrepancies are found for M_2 tidal velocity with 0.041 and 0.024 m s^{-1} for U and V respectively, while minimum errors are observed for P_1. On the other hand, the phase errors ($G_c - G_o$) between the computed and observed *U* and *V* components are found to be reasonable, with maximum phase errors of 32.9 and 32.3 degrees for the north velocity of O_1 and P_1 respectively. To obtain an evaluation of the model performance regarding horizontal and/or vertical tide, the deviations in terms of amplitude ratio and phase errors were considered. The typical value of phase error is 0 and the amplitude ratio is 1 (Deltares, 2011). It was observed that the amplitude ratio (H_c / H_o) is approximately close to 1 for all components of *U* and *V* tide, and the phase errors ($G_c - G_o$) are found to be less than 33 degrees. Statistical assessment in Table 9 shows that the *SD* of the tidal analysis is 0.01, while the *SVD* is less than 0.2. These results indicate that the tidal model (AG-Model) in terms of east and north velocities is performing well.

To study the tidal currents in the AG, the simulated tide-induced currents from the numerical model are analysed. The simulation results are analysed under flood and ebb conditions during the spring tide. The simulated tide-induced current patterns during flood and ebb are shown in Figure 9a,b. The tidal currents in general are changing

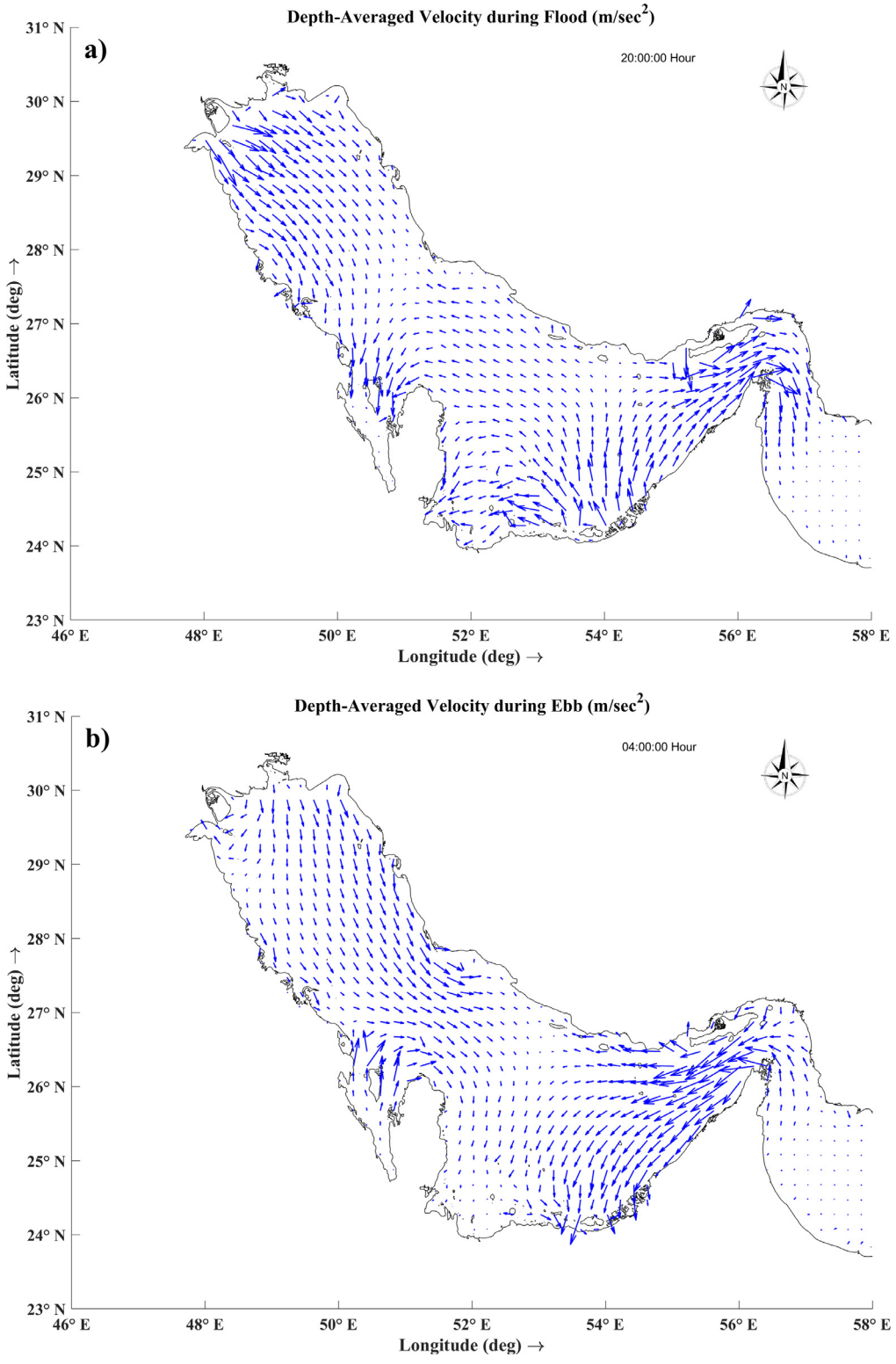

Figure 9 Depth averaged velocity during (a) flood (20:00:00 hr) and (b) ebb (04:00:00 hr) conditions.

based on the basin geometry and ocean currents of flood and ebb tides. The simulation results reveal that the current magnitude of 0.25—0.5 m s^{-1} is dominated in the AG. The highest velocities during flood tide were observed in the Strait of Hormuz, in the vicinity of the northern part, in the vicinity of Bahrain and western coast of Qatar, and in the shallow coastal areas along UAE. The maximum current velocities extend up to 0.86 m s^{-1} in the vicinity of the Strait of Hormuz and the head of the Gulf. The simulation results are comparable with the tidal simulations of Najafi and Noye, (1997) and the more recent modelling study of Mehri et al. (2021).

The simulation results suggest an intensification of currents along the north-western coast (Saudi coast) directed

Table 8 Comparison between amplitudes and phases of computed and observed tidal components of North velocities (m s^{-1}) at the Strait of Hormuz for the year 1997.

Components	H_o	H_c	G_o	G_c	$H_c - H_o$	$G_c - G_o$	H_c / H_o
M_2	0.152	0.176	34.9	49.7	0.024	14.8	1.1
S_2	0.062	0.068	69.7	81.1	0.007	11.4	1.1
N_2	0.038	0.042	18.2	32.2	0.004	14.0	1.0
K_1	0.171	0.163	204.6	221.9	-0.008	17.3	0.9
O_1	0.062	0.075	177.5	210.4	0.013	32.9	1.2
P_1	0.055	0.045	185.8	218.1	-0.010	32.3	0.8

H_o: amplitude of observed tide, G_o: phase of the observed tide, H_c: amplitude of simulated tide, G_c: phase of the simulated tide, H_c - H_o: amplitude difference, G_c - G_o: Phase difference, H_c / H_o: Amplitude ratio.

Table 9 Statistical assessment obtained from *Delft3D-TRIANA*.

Parameters	East velocities at Strait of Hormuz	North velocities at Strait of Hormuz
SD	0.01	0.01
LER	-0.04	-0.03
UER	0.04	0.03
SVD	0.18	0.19

SD: Standard deviation of tidal Analysis; **LER:** Lower extreme for residuals; **UER:** Upper extreme for residuals; **SVD:** Summed vector differences.

southward, and along the UAE shallow areas directed northward and eastward. On the other hand, maximum currents magnitude during ebb tide (0.25 m s^{-1}) is also detected in the Strait of Hormuz, and along the UAE shallow coastal waters (0.4 m s^{-1}). The simulation results reveal that the direction of tidal currents contains some variability. In the northern and central part, the tidal currents are directed southward, however, in the Strait of Hormuz and the southern part, it is opposite, causing a deviation to the tidal currents towards the south-western coast.

4. Conclusion

The current study is concerned with the simulation of tidal hydrodynamics in the AG using a vertically 2-D hydrodynamic model based on the *Delft3D* modelling system. The model is a barotropic solution forced by 13 tidal components at the open boundaries in the eastern Gulf of Oman (58°E). The model results were validated against the available water level observations at 7 locations, and data from T/P, where statistical analyses in terms of *BIAS*, *RMSD*, *IOA*, *SD*, and *SVD* parameters were considered to evaluate the numerical model. Using 13 tidal constituents along the open boundary indeed provided very good results (error 4%) compared with the previous modelling studies carried out in the Gulf, which considered only a limited number of tidal constituents to drive the models, indicating that nonlinear interactions cannot be ignored. Sensitivity analysis also showed that the model prediction based on 13 tidal constituents produces much better results than the model prediction using 4/8 tidal components at the open sea boundary. The analysis showed that the *BIAS* value varies from 0.01 to 0.1 m while, *RMS* error was found to be ranged from 0.07 to 0.23 m, with maximum discrepancies observed at Ras Tanura and Mina Sulman stations. These two stations are mainly located at marine platforms/constructions, and characterised by complex bathymetry, therefore, a small-scale high-resolution 'child' model coupled with a coarse-scale 'parent' model applying the nesting approach would improve the accuracy of predictions in such areas, as shown in different studies (e.g., Barth et al., 2005; Debreu et al., 2012). However, the *IOA* was found to be significant with p-values less than 0.0001. The *IOA* values are found to be over 0.95 for all stations, except the Qurayyah Pier station, with a value of 0.83 (Table 3). The *SD* of the tidal analysis is found close to zero, while the *SVD* is found to be 0.074, 0.269, 1.397, and 0.741 for Jask Harbour, Qurayyah, Ras Tanura, and Marjan Island stations respectively (Table 5). On the other hand, the amplitude ratio (H_c /H_o) for semidiurnal tidal constituents and diurnal constituents is found close to 1, while the phase error ($G_c - G_o$) is observed to be satisfactorily in all stations. Based on the statistical evaluation, the simulation results were analysed to generate co-tidal charts. The results showed that the semidiurnal tides generate two amphidromic points located in the northern and southern parts, around 28.25° and 24.5°N respectively, while diurnal tides generate a single amphidromic system located in the central part around 26.8°N.

The hydrodynamic model was also validated in terms of *U* and *V* velocity components in the Strait of Hormuz with a previous study by Johns et al. (2003). The amplitude ratio (H_c / H_o) is found to be close to 1 for all components of *U* and *V* tide, and the phase error ($G_c - G_o$) is found to be less than 33 degrees. The simulation showed that the highest velocities occur in the Strait of Hormuz, in the vicinity of the northern part, in the vicinity of Bahrain and western coast of Qatar, and in the shallow coastal areas along UAE. The simulation also suggests an intensification of tidal currents along the north-western coast (Saudi coast) during flood condition

and the eastern coast of Iran during ebb condition directed southward. In summary, although the AG-Model underestimates slightly high/low waters, the analysis indicates that the model can reproduce the tidal surface elevations in the AG region with very good accuracy. In the next step, the 2-D tidal model will be extended into a 3-D approach to investigate the relevant forcing mechanisms that play a major role in the circulation of the AG, including wind conditions and thermohaline fluxes.

Acknowledgment

The simulations in this work were performed at King Abdul-Aziz University's High-performance Computing Centre (Aziz super-computer) (http://hpc.kau.edu.sa). This project was funded by the Deanship of Scientific Research (DSR), King Abdulaziz University, Jeddah, under grant No. (D-086—150-1441). The authors, therefore, gratefully acknowledge DSR technical and financial support. The authors are also highly thankful to the ARAMCO Oil Company and Sea Level Centre at University of Hawaii for providing the Sea Level data.

Appendix

Table 1a, 2a, 3a and 4a.

Table 1a Comparison between amplitudes and phases of computed and observed tidal components at Jubail station.

Components	H_o	H_c	G_o	G_c	$H_c - H_o$	$G_c - G_o$	H_c / H_o	*SNR*
M_2	0.544	0.502	137.6	231.1	-0.042	93.5	0.9	1E+03
S_2	0.246	0.206	90.4	153.4	-0.040	63.1	0.8	1.9E+02
N_2	0.093	0.098	105.7	19.1	0.004	-86.6	1.0	2.8E+01
K_2	0.025	0.064	160.9	99.1	0.039	-61.8	2.6	7.2E-03
K_1	0.144	0.102	84.5	64.3	-0.042	-20.2	0.7	1.9E+02
O_1	0.144	0.119	293.1	292.4	-0.024	-0.7	0.8	2.1E+02
P_1	0.043	0.036	100.8	98.2	-0.006	-2.6	0.9	3.8E+00
Q_1	0.020	0.022	264.8	221.2	0.002	-43.6	1.1	2.3E+00

H_o: amplitude of observed tide, G_o : phase of the observed tide, H_c: amplitude of simulated tide, G_c: phase of the simulated tide, H_c - H_o: amplitude difference, G_c - G_o: Phase difference, H_c / H_o: Amplitude ratio, *SNR*: signal-to-noise ratio.

Table 2a Comparison between amplitudes and phases of computed and observed tidal components at Arabiyah Island station.

Components	H_o	H_c	G_o	G_c	$H_c - H_o$	$G_c - G_o$	H_c / H_o	*SNR*
M_2	0.365	0.336	191.2	147.8	-0.029	-43.4	0.9	2.5E+03
S_2	0.132	0.111	162.1	115.0	-0.020	-47.2	0.8	2.6E+02
N_2	0.069	0.069	61.9	15.2	-0.001	-46.7	1.0	8.4E+01
K_2	0.038	0.037	327.7	278.6	-0.001	-49.1	1.0	3.2E+01
K_1	0.189	0.150	95.8	66.3	-0.039	-29.5	0.8	1.8E+03
O_1	0.129	0.113	136.3	118.7	-0.016	-17.6	0.9	6.5E+02
P_1	0.061	0.044	98.0	67.0	-0.017	-31.0	0.7	1.8E+02
Q_1	0.022	0.021	25.3	357.8	-0.001	-27.4	1.0	2.1E+01

H_o: amplitude of observed tide, G_o: phase of the observed tide, H_c: amplitude of simulated tide, G_c: phase of the simulated tide, H_c - H_o: amplitude difference, G_c - G_o: Phase difference, H_c / H_o: Amplitude ratio, *SNR*: signal-to-noise ratio.

Table 3a Comparison between amplitudes and phases of computed and observed tidal components at Mina Sulman station.

Components	H_o	H_c	G_o	G_c	$H_c - H_o$	$G_c - G_o$	H_c / H_o	*SNR*
M_2	0.710	0.550	319.3	330.7	-0.160	11.4	0.8	5.4E+03
S_2	0.208	0.165	97.0	92.9	-0.042	-4.1	0.8	3.7E+02
N_2	0.156	0.125	6.5	17.4	-0.031	10.8	0.8	2.7E+02
K_2	0.081	0.050	252.7	249.2	-0.031	-3.5	0.6	9.5E+01
K_1	0.098	0.082	156.6	152.2	-0.016	-4.4	0.8	3.2E+02
O_1	0.065	0.056	16.4	32.2	-0.008	15.8	0.9	1.3E+02
P_1	0.036	0.022	166.1	155.2	-0.014	-10.8	0.6	4.3E+01
Q_1	0.009	0.010	60.4	79.9	0.001	19.5	1.0	2.9E+00

H_o: amplitude of observed tide, G_o: phase of the observed tide, H_c: amplitude of simulated tide, G_c: phase of the simulated tide, H_c - H_o: amplitude difference, G_c - G_o: Phase difference, H_c / H_o: Amplitude ratio, ***SNR***: signal-to-noise ratio.

Table 4a Statistical assessment obtained from *Delft3D-TRIANA*.

Parameters	Station ID		
	Jubail	*Mina Sulman*	*Arabiyah Island*
SD	0.040	0.049	0.028
LER	-0.143	-0.208	-0.099
UER	0.119	0.127	0.085
SVD	1.092	1.563	1.078

SD: Standard deviation of tidal Analysis; **LER**: Lower extreme for residuals; **UER**: Upper extreme for residuals; **SVD**: Summed vector differences.

References

Admiralty, 2012. Co-tidal atlas Persian Gulf. NP 214.

Ahmad, F., Sultan, S.A.R., 1991. Annual mean surface heat fluxes in the Arabian Gulf and the net heat transport through the Strait of Hormuz. Atmos. Ocean 29 (1), 54—61. https://doi.org/10.1080/07055900.1991.9649392

Akbari, P., Sadrinasab, M., Chegini, V., Siadatmousavi, M., 2016. Tidal constituents in the Persian Gulf, Gulf of Oman and Arabian Sea: a numerical study. Indian J. Geo-Mar. Sci. 45 (8), 1010—1016.

Al-Mahdi, A.A., Abdullah, S.S., Husain, N.A., 2009. Some features of the physical oceanography in Iraqi marine waters. Mesopotamian J. Mar. Sci. 24, 13—24.

Al-Subhi, A.M., 2010. Tide and sea level characteristics at Juaymah, west coast of the Arabian Gulf. J. King Abdulaziz Univ. Mar. Sci. 21, 133—149. https://doi.org/10.4197/Mar.21-1.8

Arakawa, A., Lamb, V.R., 1977. Computational Design of the Basic Dynamical Processes of the UCLA General Circulation Model. Methods Comput. Phys. 173—265. https://doi.org/10.1016/B978-0-12-460817-7.50009-4

Balaji, R., 2012. A case study on curtailed tidal hydrodynamic modeling along UAE coast. Int. J. Ocean Clim. Syst. 3, 45—56.

Barth, A., Alvera-Azcárate, A., Rixen, M., Beckers, J.-M., 2005. Two-way nested model of mesoscale circulation features in the Ligurian Sea. Prog. Oceanogr. 66, 171—189.

Bashir, M., 1993. Numerical modelling of tidal flows in the Arabian gulf. Brunel University, School of Information Systems, Computing and Mathematics.

Brewer, P.G., Dyrssen, D., 1985. Chemical oceanography of the Persian Gulf. Prog. Oceanogr. 14, 41—55.

Brewer, P.G., Fleer, A.P., Kadar, S., Shafer, D.K., Smith, C.L., 1978. Chemical oceanographic data from the Persian Gulf and Gulf of Oman. WHO Rep. 78, 37.

Chao, S.-Y., Kao, T.W., Al-Hajri, K.R., 1992. A numerical investigation of circulation in the Arabian Gulf. J. Geophys. Res. Ocean. 97, 11219—11236.

Debreu, L., Marchesiello, P., Penven, P., Cambon, G., 2012. Two-way nesting in split explicit ocean models: Algorithms, implementation and validation. Ocean Model. 49, 1—21.

Defant, A., 1961. In: Physical Oceanography, 1. Pergamon Press, London, 729 pp. https://doi.org/10.1017/S0025315400070089

Deltares, 2011. Delft3D-FLOW User Manual Simulation of Multi-dimensional Hydrodynamic Flows and Transport Phenomena, Including Sediments, User Manual, Hydro Morphodynamics, Version: 3.15

Egbert, G.D., Erofeeva, S.Y., 2002. Efficient Inverse Modeling of Barotropic Ocean Tides. J. Atmos. Ocean. Technol. 19, 183—204. https://doi.org/10.1175/1520-0426(2002)019⟨0183:EIMOBO⟩2.0.CO;2

Elshorbagy, W., Azam, M.H., Taguchi, K., 2006. Hydrodynamic characterization and modeling of the Arabian Gulf. J. Waterw. port, coastal, Ocean Eng. 132, 47—56.

Emery, K.O., 1956. Sediments and water of Persian Gulf. Am. Assoc. Pet. Geol. Bull. 40, 2354—2383.

Johns, W.E., Yao, F., Olson, D.B., Josey, S.A., Grist, J.P., Smeed, D.A., 2003. Observations of seasonal exchange through the Straits of Hormuz and the inferred heat and freshwater budgets of the Persian Gulf. J. Geophys. Res. 108 (12), 12—21. https://doi.org/10.1029/2003JC001881

Kämpf, J., Sadrinasab, M., 2006. The circulation of the Persian Gulf: a numerical study. Ocean Sci. 2 (1), 27—41. https://doi.org/10.5194/os-2-27-2006

Khalilabadi, M.R., 2016. Tide—surge interaction in the Persian Gulf, Strait of Hormuz and the Gulf of Oman. J. Weather 71 (10), 256—261. https://doi.org/10.1002/wea.2773

Lardner, R.W., Belen, M.S., Cekirge, H.M., 1982. Finite difference model for tidal flows in the Arabian Gulf. Comput. Math. Appl. 8 (6), 425—444. https://doi.org/10.1016/0898-1221(82)90018-9

Lardner, R.W., Lehr, W.J., Fraga, R.J., Sarhan, M.A., 1988. A model of residual currents and pollutant transport in the Arabian Gulf. Appl. Math. Model. 12, 379—390.

Madah, F., Mayerle, R., Bruss, G., Bento, J., 2015. Characteristics of tides in the Red Sea region, a numerical model study. Open J. Mar. Sci. 5, 193—209. https://doi.org/10.4236/ojms.2015.52016

Mason, E., Molemaker, J., Shchepetkin, A.F., Colas, F., McWilliams, J.C., Sangrà, P., 2010. Procedures for offline grid nesting in regional ocean models. Ocean Model 35, 1—15.

Mehri, F., Torabi Azad, M., Mansoury, D., 2021. A Hydrodynamic Model of Tidal Current in the Strait of Hormuz. Int. J. Coast. Offshore Eng. 37—45.

Mohamed, K.A., El-Dahshan, M.E., 2002. Tidal analysis and prediction of the flow characteristics around. Abu dhabi Island. WIT Trans. Eng. Sci. 36.

Najafi, H.S., 1997. Modelling tides in the Persian Gulf using dynamic nesting. Univ. Adelaide, South Australia, 145 PP.

Palacio, C., Mayerle, R., Toro, M., Jimenez, N., 2005. Modelling of flow in a tidal flat area in the south-eastern German bight. Die Küste, 69 PROMORPH, 141—174.

Perrone, T.J., 1979. Winter shamal in the Persian Gulf. Tech. Rep., Naval Environ. Predict. Res. Facil., Monterey, Calif. 79—106.

Poul, H.M., Backhaus, J., Huebner, U., 2016. A description of the tides and effect of Qeshm canal on that in the Persian Gulf using two-dimensional numerical model. Arab. J. Geosci. 9, 148.

Pous, S., Carton, X., Lazure, P., 2012. A process study of the tidal circulation in the Persian Gulf. Open J. Mar. Sci. 2, 131—140.

Pous, S.P., Carton, X., Lazure, P., 2004. Hydrology and circulation in the Strait of Hormuz and the Gulf of Oman—Results from the GOGP99 Experiment: 2. Gulf of Oman. J. Geophys. Res. Ocean. 109.

Privett, D.W., 1959. Monthly charts of evaporation from the N. Indian Ocean (including the Red Sea and the Persian Gulf). Q. J. R. Meteorol. Soc. 85, 424—428.

Pugh, D.T., 2004. Changing Sea Levels: Effects of Tides, Weather and Climate. Eos, Trans. Am. Geophys. Union 85, 468. https://doi.org/10.1029/2004EO450010

Quaresma, L.S., Pichon, A., 2013. Modelling the barotropic tide along the West-Iberian margin. J. Mar. Syst. 109, S3—S25.

Reynolds, R.M., 1993. Physical oceanography of the Gulf, Strait of Hormuz, and the Gulf of Oman—Results from the Mt Mitchell expedition. Mar. Pollut. Bull. 27, 35—59.

Roelvink, J.A., Banning, V.G., 1995. Design and development of DELFT3D and application to coastal morphodynamics. Oceanogr. Lit. Rev. 11, 925.

Roos, P.C., Schuttelaars, H.M., 2011. Influence of topography on tide propagation and amplification in semi-enclosed basins. Ocean Dyn. 61, 21—38.

Sharaf El-Din, S.H., 1988. Sea Level Variation along the Saudi Coast of the Arabian Gulf and their Relation to Meteorological Parameters. Spec. Rep. 1409.

Siddig, N.A., Al-Subhi, A.M., Alsaafani, M.A., 2019. Tide and mean sea level trend in the west coast of the Arabian Gulf from tide gauges and multi-missions satellite altimeter. Oceanologia 61 (4), 401—411. https://doi.org/10.1016/j.oceano.2019.05.003

Spall, M.A., Holland, W.R., 1991. A nested primitive equation model for oceanic applications. J. Phys. Oceanogr. 21, 205—220.

Stelling, G.S., Leendertse, J.J., 1992. Approximation of convective processes by cyclic AOI methods. Estuar. Coastal Model. 771—782.

Sultan, S.A.R., Ahmad, F., Elghribi, N.M., Al-Subhi, A.M., 1995. An analysis of Arabian Gulf monthly mean sea level. Cont. Shelf Res. 15, 1471—1482.

Thompson, E.F., Demirbilek, Z., Hadley, L.L., Rivers, P., Huff, K.E., 1994. Water Level and Current Simulation for LOTS Operations-Persian Gulf and Gulf of Oman.

Trepka, V.L., 1968. Investigation of the tides in the Persian Gulf by means of ahydrodynamic numerical model. In: Proceeding of Symposium on Mathematical Hydrological Investigations of Physical Process in the Sea, 59—63.

Verboom, G.K., Slob, A., 1984. Weakly reflective boundary conditions for two-dimensional water flow problems. 5th Int. Conf. on Finite Elements in Water Resources, June 1984, Vermont. Also Adv. Water Resour., 7.

Willmott, C.J., 1981. On the validation of models. Phys. Geogr. 2, 184—194.

Yao, F., 2008. Water mass formation and circulation in the Persian Gulf and water exchange with the Indian Ocean Ph.D. thesis. Univ. of Miami.